Electronic Research Archive

ERA, 31(10): 6303–6326.
DOI: 10.3934/era.2023319
Received: 20 June 2023
Revised: 09 September 2023
Accepted: 12 September 2023
Published: 22 September 2023

http://www.aimspress.com/journal/ERA

Research article

Research on impact reduction of flexible boundary particle damping honeycomb plate based on discrete element multi body dynamics coupling

Dike Hu[1,2], Hua Wang[2], Zijie Huang[3] and Wangqiang Xiao[3,*]

[1] Department of Aeronautics and Astronautics, Fudan University, Shanghai 200433, China
[2] Shanghai Aerospace System Engineering Research Institute, Shanghai 201109, China
[3] School of Aeronautics Engineering, Xiamen University, Xiamen 361000, China

* **Correspondence:** Email: wqxiao@xmu.edu.cn.

Abstract: The exposed platform is the main component of precision instruments such as pyrotechnic separation devices and load adapters, and its dynamic response characteristics are a key factor affecting the stability of aircraft. When the pyrotechnic separation device explodes, the exposed platform will be subjected to high-frequency, transient and high-order pyrotechnic impacts. High order pyrotechnic impacts can easily cause damage to sensitive components in onboard equipment, resulting in incalculable losses. Filling the honeycomb core cavity inside the exposed platform with a flexible boundary particle damper can effectively attenuate the pyrotechnic impact load after experiencing a large number of discontinuous structures. A numerical model of a flexible boundary particle damper and an exposed platform honeycomb panel was established through the coupling of discrete element and multi body dynamics. The effects of particle material, particle size, filling rate and flexible boundary film thickness on the impact reduction performance of the flexible boundary particle damper were analyzed, and the optimal characteristic parameters of the flexible boundary particle damper were obtained. The impact test was conducted on the honeycomb panel of the exposed platform using a light gas gun impact experiment, verifying the impact reduction effect of the flexible boundary particle damper and the accuracy of the numerical model. Finally, a pyrotechnic impact experiment was conducted on the exposed platform honeycomb panel with the optimal parameter flexible boundary particle damper. The experimental results showed that the impact reduction effect of the flexible boundary particle damper with this parameter reached 55.52%.

Keywords: discrete element multibody dynamics coupling; particle damping; impact reduction

1. Introduction

The exposed platform is an important structure used on spacecraft to carry precision instruments such as pyrotechnic separation devices, connectors, four-way valves and liquid floats. When the pyrotechnic separation device on the platform explodes, it can generate high-frequency and high-order pyrotechnic impacts [1] to complete actions such as star rocket separation [2–3] and valve opening and closing [4]. The exposed platform adopts a honeycomb core structure internally to reduce the overall weight of the platform, while ensuring the stability of the explosion unlocking action and having certain impact energy absorption characteristics.

When the pyrotechnical separation device explodes, it will generate pyrotechnical shock response with high frequency, transient and high-order characteristics on the spacecraft, accompanied by the release of structural preload strain energy [5–7] and the impact between components. This impact has little impact on the main structure of the spacecraft, but often causes damage to sensitive components in the on-board equipment [8]. When the load compartment exposes the platform to a pyrotechnic impact, the precision instruments on the platform will withstand a larger impact load. If the impact load is too large, it will generate high-strength stress inside the structure [9–11], causing brittle parts to break and causing serious consequences [12,13]. Therefore, controlling the impact load generated by the pyrotechnic separation device and reducing the pyrotechnic impact load borne by the precision instruments on the platform has significant theoretical significance and practical value.

Adding shock isolation devices to the shock transmission path is an effective means of controlling the impact load of pyrotechnics, and many scholars have conducted in-depth research on the isolation devices of pyrotechnics. The Argentine National Committee on Space Activities [14] has designed an impact isolation device composed of glass fiber, stainless steel and magnesium alloy layers. The device forms an isolation layer between the main structure and the pyrotechnic separation device to reduce the impact of pyrotechnic explosions. Later, the SAC-B satellite was used for pyrotechnic impact experiments to achieve good impact reduction effects. Irvine [15] combines metal mesh materials and silicone rubber pads to form a pyrotechnic shock load absorption device for shock isolation of key instruments. The results show that the device can effectively absorb pyrotechnic loads and slowly release them. Garcia et al. [16] adjusts the stiffness of the impact load transfer interface through a combination of metal gaskets and silicone rubber to achieve rapid attenuation of pyrotechnic loads. Ariane-5 rocket experiments have shown that the device has a good impact reduction effect. From the above research, it can be seen that most of the current methods to reduce the impact load of pyrotechnics are to add isolation layers on the transmission path. Although this approach can effectively reduce the amplitude of pyrotechnic response, it will have a significant impact on the connection stiffness.

In response to the problem of excessive impact load caused by pyrotechnics, we propose for the first time the application of flexible boundary particle dampers in the study of impact reduction on exposed platforms. The interior of the exposed platform of the load compartment is composed of a large number of honeycomb holes. A large number of flexible boundary particle dampers are filled in the honeycomb holes of the exposed platform, increasing the number of discontinuous nodes that the thermal shock stress wave passes through during the transmission process, which can effectively

reduce the impact response amplitude of the target area. Furthermore, the flexible constraint layer of the flexible boundary particle damper can effectively absorb the energy generated by the inelastic collision between particles, and effectively reduce the vibration and impact transmitted from the traditional rigid constrained damping structure back to the main system. Especially in space microgravity, the flexible constraint layer outside the particles in the flexible boundary particle damping technology can effectively increase the collision efficiency between particles. Therefore, flexible boundary particle damping technology has good applicability in pyrotechnic impact environments.

In response to the research demand for reducing impact on the exposed platform of the load compartment, a discrete element multi body dynamic coupling analysis was conducted on the characteristic model of the honeycomb panel of the exposed platform to obtain the optimal parameters of the flexible boundary particle damper. Impact experiments were conducted on the exposed platform, and the results showed that the flexible boundary particle damper effectively reduced the pyrotechnic impact on the honeycomb panel of the exposed platform, providing important technical support for the field of pyrotechnic impact protection.

2. Theoretical model

2.1. Discrete element analysis

We design a honeycomb panel impact reduction system based on flexible boundary particle damping technology for the exposed platform honeycomb panel of the load compartment as the research object. The main research content of the flexible boundary particle damping system is to establish the particle system in the flexible boundary particle damping system through the discrete element software EDEM, and to establish the dynamic model of the flexible boundary film and exposed platform honeycomb plate based on the finite element flexible body method. The influence of particle parameters such as particle size, particle filling rate, particle material, etc. on the impact reduction effect is analyzed, and the optimal parameters of the flexible boundary particle damping system are determined, Finally, the impact reduction effect of the flexible boundary particle damping system based on the exposed platform was verified through experiments.

This article adopts a soft ball model, and after introducing the elastic and damping coefficients, the contact force between particles can be calculated through the overlap [17] between elements. Then, the motion form of the dispersed body can be obtained through central difference iteration [18]. The motion equations of any particle in the particle system at a certain moment when the honeycomb panel of the exposed platform is impacted:

$$\begin{cases} m_i \ddot{p}_i = \sum_{j=1}^{u_i} (F_{nij} + F_{sij}) \\ I_i \ddot{\varphi}_i = \sum_{j=1}^{u_i} T_{ij} \end{cases} \tag{1}$$

In the equation, m_i is the particle mass; I_i is the particle moment of inertia; p_i, φ_i is the displacement and angular displacement vector of the particle, respectively; F_{nij}, F_{sij} is the normal and tangential contact force between particle i and unit j; T_{ij} is the torque generated by the tangential contact force; u_i represents the number of units that come into contact with unit i at a certain moment. Based on Hertz contact theory, the contact force model of the honeycomb core damping system is

shown in Figure 1.

Contact force between particles:

$$F_{nij} = k_n \delta_n + 2\xi \sqrt{\frac{m_i m_j}{m_i + m_j} k_n \dot{\delta}_n} \quad \text{（P-P）} \tag{2}$$

$$F_{sij} = -\mu F_{nij} \frac{\dot{\delta}_s}{|\dot{\delta}_s|} \quad \text{（P-P）} \tag{3}$$

In the equation, δ_n, $\dot{\delta}_n$ represents the displacement and velocity of particle i relative to unit j respectively; μ is the friction coefficient between particles; δ_s is the tangential velocity of particle i relative to unit j; k_n is the normal elastic coefficient in the contact model.

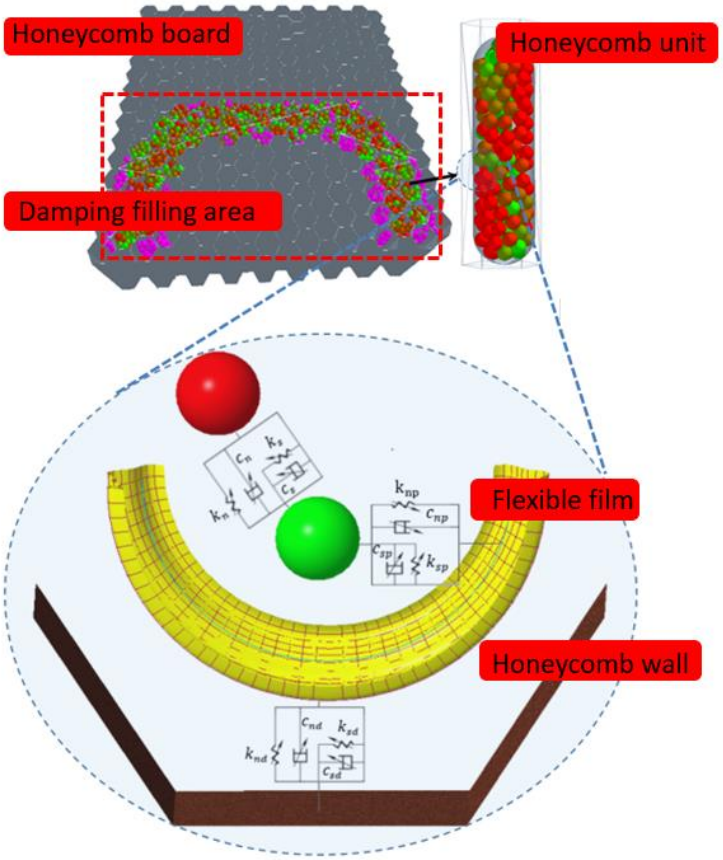

Figure 1. Contact model.

We fill a flexible boundary particle damper with particles of a single material and particle size. According to Hertz contact theory, the elastic coefficient k_n and k_s can be determined as:

$$k_n = \frac{2}{3}\left(\frac{1-v^2}{E}\right)\left(\frac{2}{R}\right)^{-\frac{1}{2}} \quad \text{（P-P）} \tag{4}$$

$$k_s = \frac{1-v}{1-0.5v} k_n \quad \text{（P-P）} \tag{5}$$

In the formula, E and v are the elastic modulus and Poisson's ratio of the contact element, respectively; R is the particle radius.

In the critical damping state, the mechanical energy decay rate is the fastest, at which point the critical normal damping coefficient C_n and tangential damping coefficient C_s are:

$$\begin{cases} c_n = 2\sqrt{\bar{m}k_n} \\ c_s = 2\sqrt{\bar{m}k_s} \end{cases} \tag{6}$$

In the equation, $\bar{m}$ is the equivalent mass of the contact unit.

2.2. Multi body dynamics analysis

There are various contact models in multi body dynamics [19], such as flexible line to flexible surface contact, flexible surface to ball contact, flexible line to flexible line contact and flexible surface to flexible surface contact. We use flexible surfaces in contact with flexible surfaces. The contact model between the flexible membrane and the honeycomb wall is shown in Figure 2.

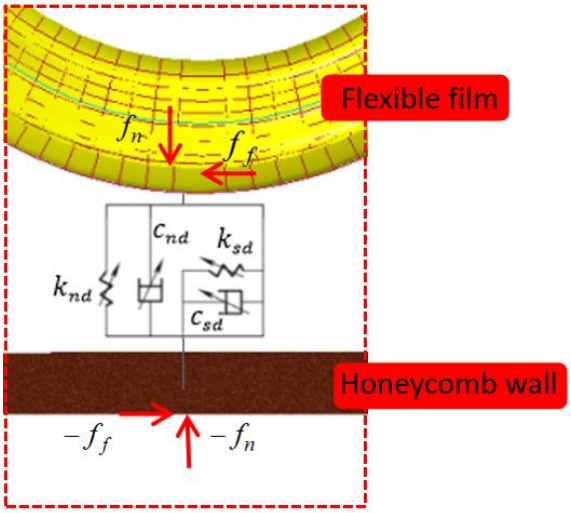

Figure 2. Flexible body contact model.

Contact force between flexible boundary film and particles:

$$f_{n1} = k_{np}\delta^{m_1} + c_{np}\delta^{m_2}\dot{\delta}\left|\dot{\delta}\right|^{(m_3-1)} \quad \text{（P-F）} \tag{7}$$

Contact force between flexible boundary film and honeycomb wall:

$$f_{n2} = k_{nd}\delta^{m_1} + c_{nd}\delta^{m_2}\dot{\delta}\left|\dot{\delta}\right|^{(m_3-1)} \quad \text{（F-D）} \tag{8}$$

Among them, δ is the longitudinal tangential displacement of two contact elements, k_{np} and k_{nd} are the contact stiffness, c_{np} and c_{nd} are the damping coefficient, m_1 is the stiffness index, m_2 is the gap index, m_3 is the damping index.

The formula for calculating friction force is:

$$f_{f1} = \mu(v)|f_{n1}| \quad \text{（P-F）} \tag{9}$$

$$f_{f2} = \mu(v)|f_{n2}| \quad \text{（F-D）} \tag{10}$$

Among them, friction coefficient μ related to relative velocity and depends on the values of static threshold velocity, dynamic threshold velocity and static friction coefficient. When the relative velocity is less than the static threshold velocity, the value of the friction coefficient is obtained through velocity interpolation. When the relative velocity is between the static threshold velocity and the dynamic threshold velocity, the friction coefficient is between the static friction coefficient and the dynamic friction coefficient. When the relative velocity is greater than the dynamic threshold velocity, the value is the dynamic friction coefficient. In the above equation, P-P represents particles and particles, P-F represents particles and flexible membranes and F-D represents flexible membranes and honeycomb walls.

In flexible body modeling, the model elements are divided, the relative displacement of flexible boundary membrane nodes is defined as a variable, and the motion equation of the model is established. The principle of solving multi body dynamics is shown in Figure 3, the relative rotation and relative displacement at the flexible node are used to express the motion of the flexible body, while the flexible body uses the absolute coordinate method to obtain the node coordinates by obtaining the slope and displacement at the node. The shape function is used to express the elastic deformation of the flexible body, so that the dynamic response results of the flexible body can be obtained without multiple operations of the structural matrix during the solving process.

The position changes of nodes on the boundary membrane can be expressed by the following formula:

$$r = r_0 + A(s_p + u_p) \tag{11}$$

r is the position vector of the node of the boundary film in the absolute coordinate system $X-Y-Z$, r_0 is the position vector of the origin of the relative coordinate system in the absolute coordinate system $X-Y-Z$, s_p is the position vector of the node in the relative coordinate system when the boundary film is not deformed, u_p is the relative deformation vector and A is the Direction cosine matrix of the boundary film node when the spatial coordinate transformation operation occurs.

The relative velocity and virtual displacement of any node on the boundary membrane can be expressed as:

$$Y = \begin{bmatrix} \dot{r}' \\ \omega' \end{bmatrix} = \begin{bmatrix} A^T \dot{r} \\ A^T \omega \end{bmatrix} \tag{12}$$

$$\delta Z = \begin{bmatrix} \delta r' \\ \delta \pi' \end{bmatrix} = \begin{bmatrix} A^T \delta r \\ A^T \delta \pi \end{bmatrix} \tag{13}$$

A is the direction transformation matrix from the relative coordinate system to the absolute coordinate system of the boundary film.

The relative deformation of boundary membrane nodes i and $i-1$ can be expressed as:

$$r_i = r_{(i-1)} + A_{(i-1)}(s'_{(i-1)i0} + u'_{(i-1)i}) \tag{14}$$

The relative angular velocity of boundary membrane nodes can be expressed as:

$$\omega'_i = A^T{}_{(i-1)i}\omega'_{i-1} + A^T{}_{(i-1)i}H^T{}_{(i-1)i}\dot{q}_{(i-1)i} \tag{15}$$

By taking the derivative of the equation, the acceleration of the boundary membrane node can be obtained. Through the above calculation, the dynamic parameters of the nodes on the boundary membrane can be accurately obtained. The multi body dynamic flexible body modeling method can accurately analyze the dynamic response of flexible bodies by repeatedly calculating the structural matrix [20] and analyzing the contact and collision between flexible bodies.

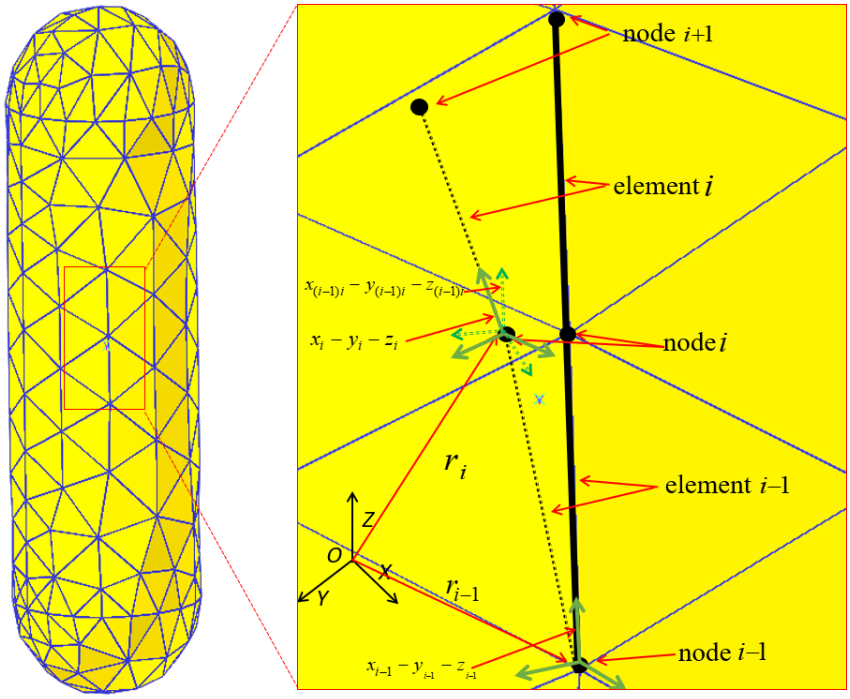

Figure 3. Principle of solving multi body dynamics.

3. The influence of characteristic parameters on impact reduction characteristics

3.1. Explosive shock load and boundary condition loading

The pyrotechnic shock load has the characteristics of high frequency, transient, broadband and high structural driving impedance. For the simulation of pyrotechnic load in coupling analysis, it cannot be simulated with a half sine wave with insufficient high-frequency components. By setting a

small ball in the multi body dynamics software to simulate the pyrotechnic environment by high-speed impact on the excitation point of the model, the acceleration time domain curve of the excitation point is shown in Figure 4, which conforms to the provisions of the national military standard GJB150A for pyrotechnic impact load.

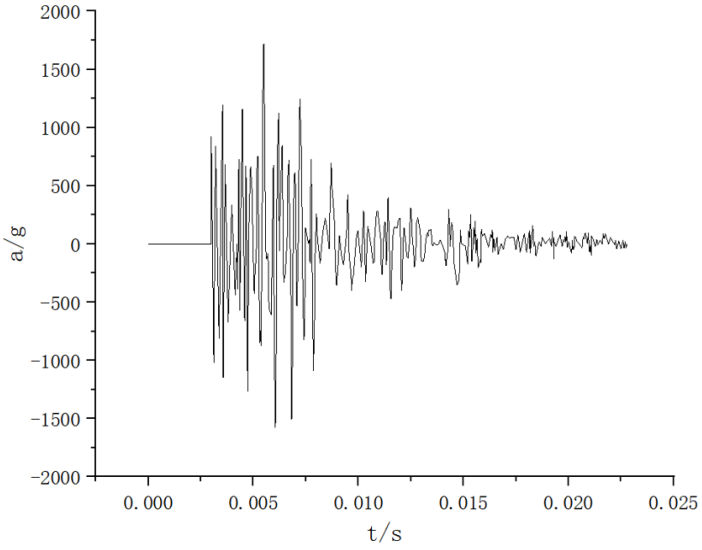

Figure 4. Impact load acceleration time history.

The exposed platform honeycomb panel is made of aluminum material, and the flexible boundary membrane material model is LVF200G278V. The simulation model is loaded through material properties [21], and the specific material parameters are shown in Table 1.

Table 1. Material parameters of honeycomb aluminum and flexible boundary film.

	Young's modulus	Density	Poisson's ratio
Aluminum honeycomb	70000MPa	2.71g/ mm^3	0.33
Flexible film	2.35 MPa	1.13g/ mm^3	0.475

The contact type adopts Flexsurface to Flexsurface, and the contact type algorithm is based on the penalty function. The collision action is decomposed into multiple incremental steps, and the dynamic parameters such as penetration and contact force are calculated by retrieving the collision behavior between each incremental step [22]. Among them, the time step parameter is 8×10^{-5} s, the specific contact parameters are shown in Table 2.

Table 2. Contact parameters of honeycomb wall and flexible boundary film.

Contact stiffness coefficient	Damping coefficient	Dynamic friction factor	Maximum penetration depth	Boundary buffer scale
10	1×10^{-4}	0.49	0.1 mm	0.5 mm

After setting the contact parameters, set the response point in the output module. The response point is located in the upper right corner of the honeycomb board, which corresponds to the precise instrument point of the exposed platform honeycomb board. The schematic diagram of the model is shown in Figure 5. Figure 5 (left) shows the modeling of honeycomb panels in a multi body dynamic system, and Figure 5 (right) shows the experimental diagram of honeycomb panels. Among them, ① represents the area where the pyrotechnic separation device is located, and ② represents the damping filling area.

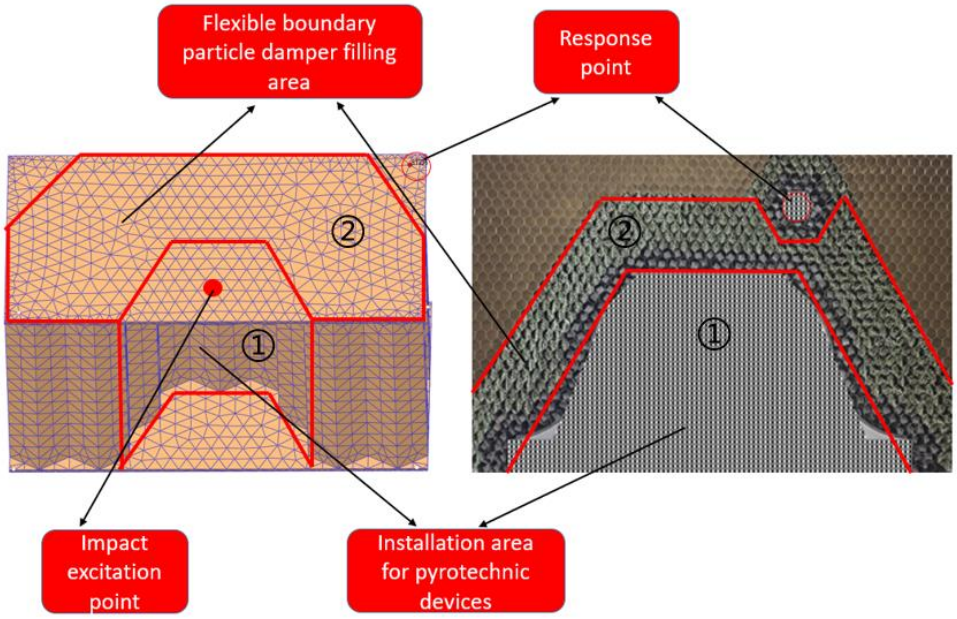

Figure 5. Model area division and response point location.

3.2. Particle material optimization

Particle material is a key factor affecting the impact reduction performance of flexible boundary particle damping systems. Different particle materials have different densities, shear moduli, Poisson's ratios and elastic recovery coefficients, and these intrinsic parameters of the materials play a crucial role in the impact reduction performance of flexible boundary particle damping systems. The different densities of particle materials can affect the forces generated during particle collisions within the flexible boundary particle damping system. Particle materials with different Poisson's ratios and shear moduli can affect the particle collision posture within the flexible boundary particle damping system. Particle materials with different recovery factors can affect the collision frequency of particles within the flexible boundary particle damping system. The intrinsic parameters of the particle material mentioned above have a significant impact on the impact reduction performance of the flexible boundary particle damper. Fill the flexible boundary particle damper with particles made of iron based alloy, ceramic based material, tungsten based alloy material and lead based alloy material for simulation analysis. The particle size is 2 mm, the filling rate is 90% and the flexible boundary film thickness is 2 mm. The particle material parameters [23] are shown in Table 3. Apply impact loads to the exposed platform honeycomb panels loaded with flexible boundary particle dampers of different

materials for numerical simulation calculations. The honeycomb panels with flexible boundary particle dampers of different particle materials are shown in Figure 6.

Table 3. Particle material parameters.

	iron base alloys	Ceramic base	tungsten-base alloy	Lead based alloy
density（g/cm^3）	7.87	2.22	19.3	10.22
shear modulus (G/Pa)	77.5	8.8	456	4.9
Poisson's ratio	0.291	0.25	0.28	0.42
Elastic coefficient of restitution	0.3	0.3	0.28	0.08

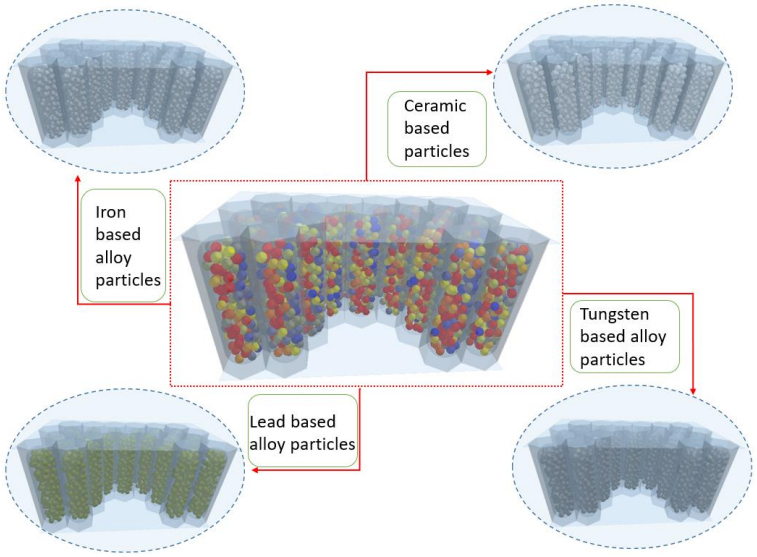

Figure 6. Flexible boundary particle dampers with different particle materials.

We perform numerical analysis on honeycomb panels adapted to flexible boundary particle dampers of different materials, loading contact parameters and impact loads. By conducting dynamic response calculations on the honeycomb panel, the acceleration time curve was obtained at the target point. The data of the acceleration time curve was imported into the impact response spectrum conversion program in MATLAB, and the acceleration time curve was converted into an impact response spectrum. The impact response spectrum is shown in Figure 7. Through the analysis of the impact response spectrum, it can be seen that the maximum peak value of the impact response spectrum of the exposed platform honeycomb panel without the addition of a flexible boundary particle damper is 4947.15 g under load. When the particle material of the flexible boundary particle damper is iron based alloy, the maximum peak value of the impact response spectrum of the exposed platform honeycomb panel is 2181.2 g, with a decrease of 55.91%. When the particles of the flexible boundary particle damper are made of ceramic substrate, the maximum peak value of the impact response spectrum of the exposed platform honeycomb panel is 3591.63 g, with a reduction of 27.4%. When the particle material of the flexible boundary particle damper is tungsten based alloy, the maximum peak value of the impact response spectrum of the exposed platform honeycomb panel is 2478.03 g, with a decrease of 49.91%. When the particle material of the flexible boundary particle damper is lead

based alloy, the maximum peak value of the impact response spectrum of the exposed platform honeycomb panel is 3916.66 g, with a reduction of 20.83%.

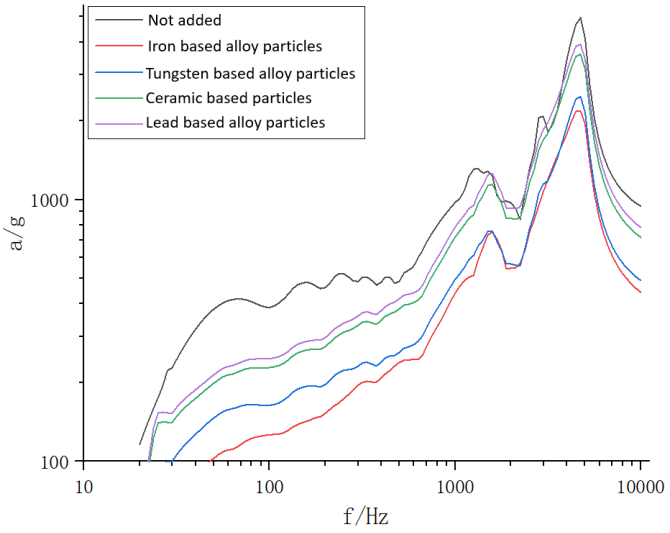

Figure 7. Impact response spectra of flexible boundary particle dampers with different particle materials installed.

According to the simulation results, among the flexible boundary particle dampers made of various materials, iron based alloys have the best impact effect, followed by tungsten based alloys and ceramic particles and lead based alloy particles have poor impact effects. Furthermore, compared to tungsten based alloys, which rank second in terms of impact reduction effect, iron based materials have lower density and better impact reduction cost-effectiveness. Therefore, in the selection of particle media for flexible boundary particle damping systems, iron based alloys are prioritized.

3.3. Particle size optimization

Particle size is an important characteristic parameter that affects the impact reduction performance of a flexible boundary particle damping system. Different particle sizes affect the number of collisions and the force between colliding particles in the entire particle system. The existence of particle systems lies between solid and liquid states. When the particle size is large, it exhibits physical properties similar to that of solid states, and the force generated by collisions during the excitation process of the particle system will increase; When the particle size is small, the particle system will exhibit liquid like physical properties, exhibiting fluid fluidity. In this state, the number of collisions generated by the particle system due to excitation will increase. Therefore, the selection of particle size is by no means as large as possible or as small as possible, and its optimal value must be determined through numerical calculations.

By filling the flexible boundary particle damper with particles of different particle sizes (as shown in Figure 8) and applying impact loads, the particle size values are 1, 1.5, 2, 2.5, 3 and 3.5 mm, respectively. The particle material selection is the iron based alloy with the best effect in the previous coupling simulation. The filling rate of the flexible boundary particle damper is set to 90%, and the flexible boundary film thickness is 0.2 mm. Through discrete element multi body dynamics coupling simulation, the impact response spectrum results of honeycomb panels with flexible boundary particle dampers with

different particle sizes were obtained. The impact response spectrum results are shown in Figure 9.

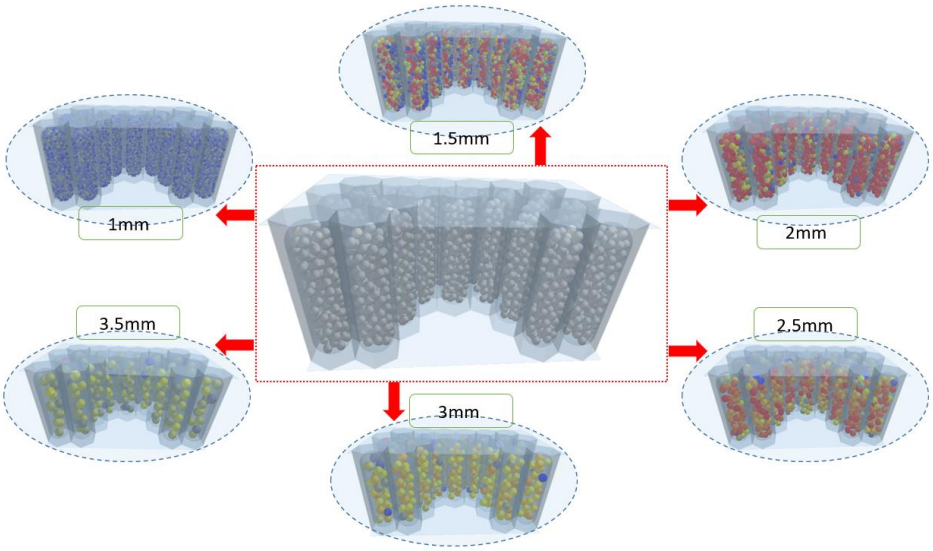

Figure 8. Flexible boundary particle damper filled with different particle sizes.

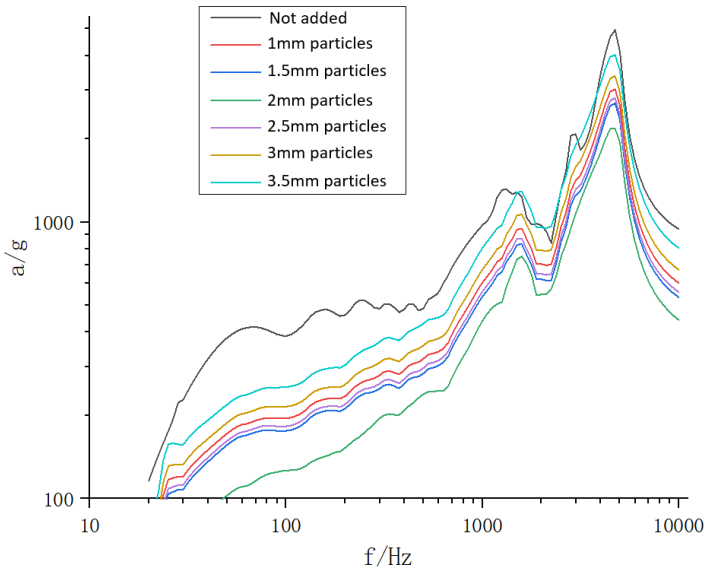

Figure 9. Impact response spectrum of installing flexible boundary particle dampers with different particle sizes.

Through the analysis of the impact response spectrum, it can be seen that the maximum peak value of the impact response spectrum of the exposed platform honeycomb panel without the addition of a flexible boundary particle damper is 4947.15 g under load. When the particle size of the flexible boundary particle damper is 1mm, the maximum peak value of the impact response spectrum of the exposed platform honeycomb panel is 3023.2 g, with a decrease of 38.89%. When the particle size of the flexible boundary particle damper is 1.5 mm, the maximum peak value of the impact response spectrum of the exposed platform honeycomb panel is 2690.75 g, with a reduction of 45.61%. When the particle size of the flexible boundary particle damper is 2 mm, the maximum

peak value of the impact response spectrum of the exposed platform honeycomb panel is 2181.2 g, with a reduction of 55.91%. When the particle size of the flexible boundary particle damper is 2.5 mm, the maximum peak value of the impact response spectrum of the exposed platform honeycomb panel is 2807.01 g, with a reduction of 43.26%. When the particle size of the flexible boundary particle damper is 3 mm, the maximum peak value of the impact response spectrum of the exposed platform honeycomb panel is 3368.02 g, with a reduction of 31.92%. When the particle size of the flexible boundary particle damper is 3.5 mm, the maximum peak value of the impact response spectrum of the exposed platform honeycomb panel is 4022.53 g, with a reduction of 18.69%. Therefore, when the particle size is 2 mm, the flexible boundary particle damper has the best impact reduction effect.

3.4. Optimization of particle filling rate

The particle filling rate is an important characteristic parameter of a flexible boundary particle damping system. The filling rate affects the flow state of the particle system in the flexible boundary particle damper chamber, thereby affecting the final impact reduction performance. During the process of changing particle filling rate from low to high, the equivalent viscosity coefficient inside the particle system will increase from small to large, leading to the flow state of particles changing from inertial flow in a low viscosity state to elastic flow in a high viscosity state. When the particle filling rate inside the flexible boundary particle damping system is low, the motion flow state of the particle system under external excitation is inertial flow. Due to the small viscous force between particles, the overall damping effect of the particle system is mainly manifested in collision. When the particle filling rate inside the flexible boundary particle damping system is high, the motion flow state of the particle system under external excitation is elastic flow. Due to the large viscous force between particles, the overall damping effect of the particle system is mainly composed of a force chain composed of viscous forces between particles, which mainly manifests as deformation and recombination of the force chain, accompanied by shear and friction work b.

Apply impact loads to honeycomb panels with flexible boundary particle dampers adapted to different filling rates, with filling rates of 60, 70, 80, 85, 90, 95 and 98%, respectively. Among them, the selection of particle material and particle size is the 2 mm iron based alloy particle with the best impact reduction performance mentioned earlier, and the flexible boundary film thickness is 0.2 mm. Simulate and analyze the exposed platform honeycomb panel to obtain the impact response spectrum results. The simulation cloud map and impact response spectrum results are shown in Figures 10 and 11.

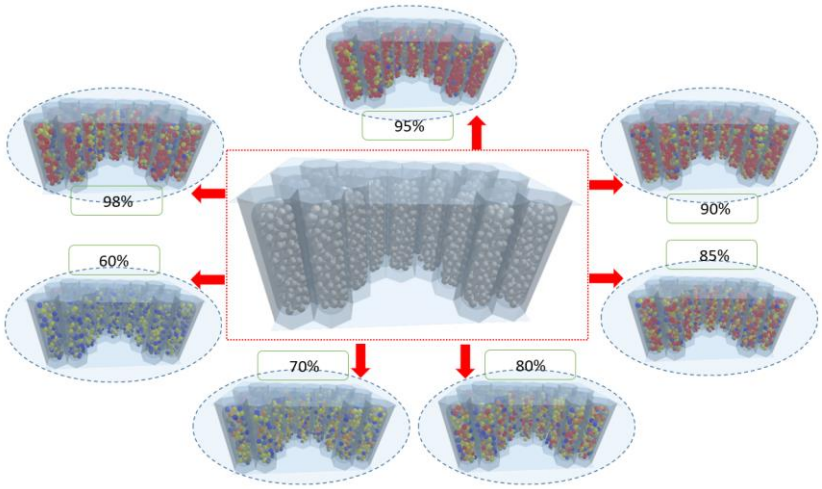

Figure 10. Flexible boundary particle dampers with different filling rates.

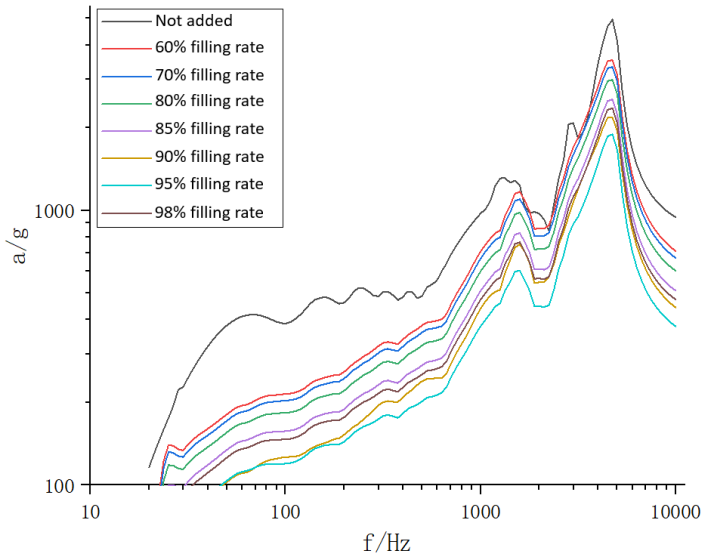

Figure 11. Impact response spectrum of flexible boundary particle dampers with different filling rates installed.

Through the analysis of the impact response spectrum, it can be seen that when the filling rate of the flexible boundary particle damper is 60%, the maximum peak of the impact response spectrum of the exposed platform honeycomb panel is 3529.3 g, with a decrease of 28.66%. When the filling rate of the flexible boundary particle damper is 70%, the maximum peak value of the impact response spectrum of the exposed platform honeycomb panel is 3328.44 g, with a reduction of 32.72%. When the filling rate of the flexible boundary particle damper is 80%, the maximum peak value of the impact response spectrum of the exposed platform honeycomb panel is 2990.06 g, with a reduction of 39.56%. When the filling rate of the flexible boundary particle damper is 85%, the maximum peak value of the impact response spectrum of the exposed platform honeycomb panel is 2539.37 g, with a reduction of 48.67%. When the filling rate of the flexible boundary particle damper is 90%, the maximum peak value of the impact response spectrum of the exposed platform honeycomb panel is 2181.2 g, with a reduction of 55.91%. When the filling rate of the flexible boundary particle damper is 95%, the maximum peak value of the impact response spectrum of the exposed platform honeycomb panel is 1891.79 g, with a reduction of 61.76%. When the filling rate of the flexible boundary particle damper is 98%, the maximum peak value of the impact response spectrum of the exposed platform honeycomb panel is 2358.8 g, with a reduction of 52.32%. Therefore, when the particle filling rate is 95%, the flexible boundary particle damper has the best impact reduction effect.

3.4. Optimization of flexible boundary film thickness

The essential difference between flexible boundary particle damper technology and particle damping technology is that it has a flexible boundary film that wraps particles. Through the flexible boundary film, the particle system inside it is flexibly constrained, allowing particles to efficiently collide and friction when impacted. When the flexible boundary particle damper is subjected to impact excitation, its flexible constraint layer can effectively absorb the energy generated by the inelastic

collision between particles, and effectively reduce the impact energy transmitted back to the main system. At the same time, considering the impact of microgravity in space, the collision and friction efficiency of particles in the traditional particle damping technology will be greatly reduced, but the flexible boundary film in the flexible boundary particle damping technology can effectively increase the collision efficiency between particles.

Adapt flexible boundary particle dampers with different thicknesses of boundary membranes (as shown in Figure 12) and apply impact loads, with boundary membrane thicknesses of 0.1, 0.2, 0.3, 0.4 and 0.5 mm, respectively. Among them, the particle material is selected as the iron based alloy with the best effect in the coupling simulation mentioned earlier. The filling rate of the flexible boundary particle damper is set to 95%, and the particle size is selected as 2 mm. Conduct coupling simulation analysis on the honeycomb panel of the exposed platform, and obtain the impact response spectrum results as shown in Figure 13.

Through the analysis of the impact response spectrum, it can be seen that when the film thickness of the flexible boundary particle damper is 0.1 mm, the maximum peak value of the impact response spectrum of the exposed platform honeycomb panel is 2244.52 g, with a reduction of 54.63%. When the film thickness of the flexible boundary particle damper is 0.2mm, the maximum peak value of the impact response spectrum of the exposed platform honeycomb panel is 1891.79 g, with a reduction of 61.76%. When the film thickness of the flexible boundary particle damper is 0.3 mm, the maximum peak value of the impact response spectrum of the exposed platform honeycomb panel is 2121.34 g, with a reduction of 57.12%. When the film thickness of the flexible boundary particle damper is 0.4 mm, the maximum peak value of the impact response spectrum of the exposed platform honeycomb panel is 2415.69 g, with a reduction of 51.17%. When the film thickness of the flexible boundary particle damper is 0.5 mm, the maximum peak value of the impact response spectrum of the exposed platform honeycomb panel is 2633.37 g, with a reduction of 46.77%. Therefore, when the film thickness is 0.2 mm, the flexible boundary particle damper has the best impact reduction effect.

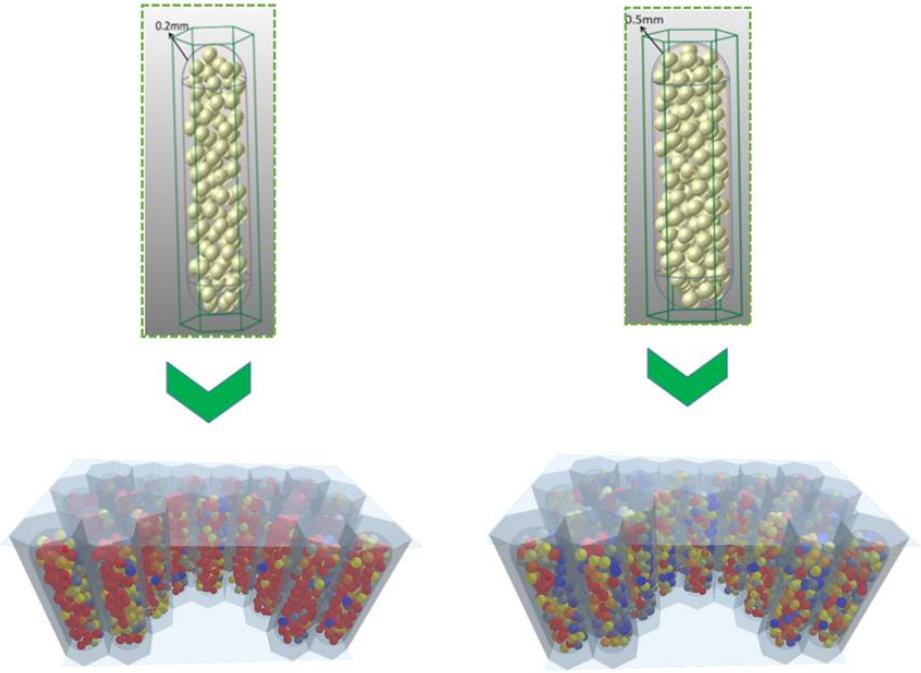

Figure 12. Flexible boundary particle dampers with different film thicknesses.

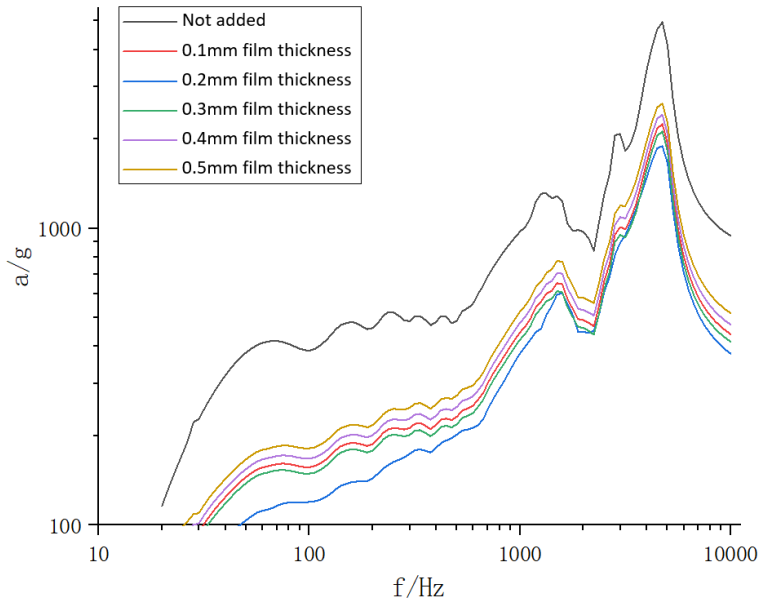

Figure 13. Impact response spectrum of flexible boundary particle dampers with different film thicknesses installed.

4. Exposed platform impact test

In order to verify the impact reduction effect of the flexible boundary particle damping system, an exposed platform impact test bench based on a light gas gun was designed to test its impact response. The impact testing system mainly includes light gas guns, INV signal acquisition system from Beijing Dongfang Institute, acceleration sensors, DASP signal analysis software, etc. The schematic diagram of the impact reduction test is shown in Figure 14.

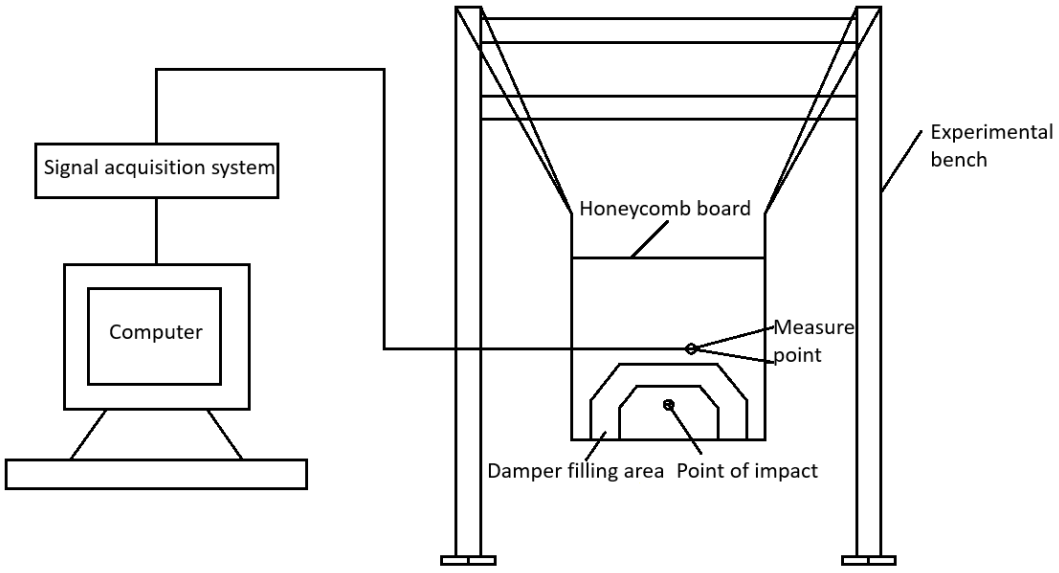

Figure 14. Schematic diagram of the test bench.

In the experiment, the exposed platform is suspended on the suspension frame with flexible ropes, so that the exposed platform is in an environment similar to space microgravity. The experiment first subjected the exposed platform without the installation of a flexible boundary particle damper to impact loading, and measured the impact response spectrum of the exposed platform without the installation of a flexible boundary particle damper. Subsequently, impact experiments were conducted on an exposed platform filled with flexible boundary particle dampers to obtain the impact response spectrum of the exposed platform after installing the flexible boundary particle damper. The installation method of flexible boundary particle dampers is to install around the impact excitation point, with a width of 30 mm. The number of filled flexible boundary particle dampers is 375 and the total weight is about 1400 g. The light gas gun is shown in Figure 15(a), the exposed platform is shown in Figure 15(b) and the internal view of the exposed platform without the installation of flexible boundary particle dampers is shown in Figure 15(c). The internal diagram of the exposed platform with flexible boundary particle dampers installed is shown in Figure 15(d).

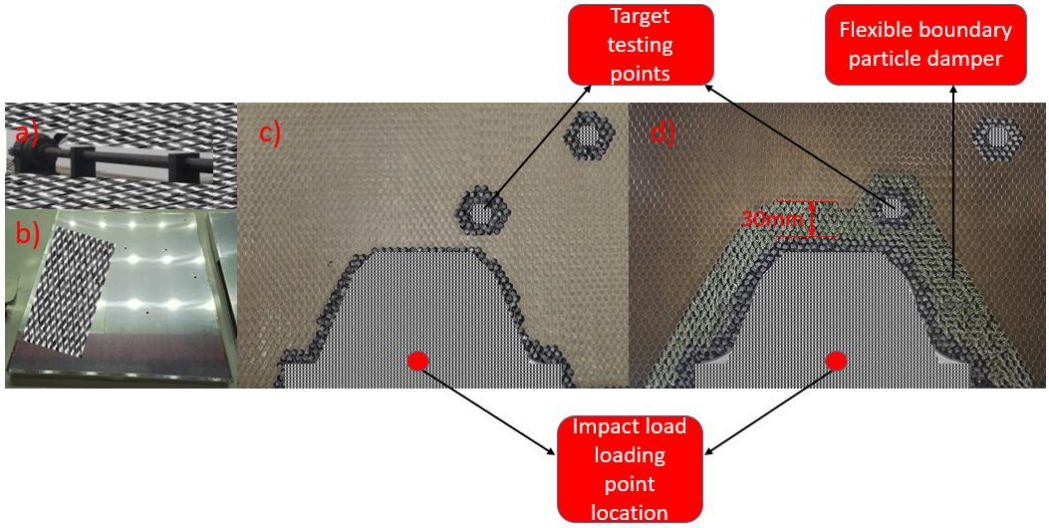

Figure 15. Exposed platform impact experiment.

4.1. Verification of particle materials

In this section, we investigate the influence of different particle materials on the impact reduction effect of flexible boundary particle dampers. By filling a 30 mm wide flexible boundary particle damper in an exposed platform honeycomb panel and applying an impact load, dynamic response results are obtained at the target point where the precision instrument is located. Five working conditions were designed for the experiment, and exposure platforms without flexible boundary particle dampers and with flexible boundary particle dampers filled with different particle materials were tested. The particle types are iron based particles, tungsten based particles, ceramic based particles and lead based alloy particles. Through impact experiments on the exposed platform, the influence of different particle materials on the impact reduction effect of flexible boundary particle dampers is explored. Among them, the other parameters of the flexible boundary particle damper are the same, with a particle size of 2 mm, a particle filling rate of 95% and a flexible boundary film thickness of 0.2 mm.

Through impact load excitation, the maximum peak of the impact response spectrum at the target point of the exposed platform without the installation of a flexible boundary particle damper was measured to occur in the frequency range of 3000–4000 Hz, with a maximum peak of 4211.91 g. When the particle material of the installed flexible boundary particle damper is lead based alloy, the maximum peak value of the impact response spectrum of the exposed platform under impact load excitation is 3443.24 g, which is 18.25% lower than the maximum peak value of the impact response spectrum without the flexible boundary particle damper installed. When the particle material of the installed flexible boundary particle damper is ceramic based, the maximum peak value of the impact response spectrum of the exposed platform under impact load excitation is 3144.61 g, which is 25.34% lower than the maximum peak value of the impact response spectrum without the flexible boundary particle damper installed. When the particle material of the installed flexible boundary particle damper is tungsten based alloy, the maximum peak value of the impact response spectrum of the exposed platform under impact load excitation is 2288.33 g. Compared with the maximum peak value of the impact response spectrum without the flexible boundary particle damper installed, the impact reduction effect reaches 45.67%. When the particle material of the flexible boundary particle damper installed is iron based alloy, the maximum peak value of the impact response spectrum of the exposed platform under impact load excitation is 1763.53 g. Compared with the maximum peak value of the impact response spectrum without the flexible boundary particle damper installed, the impact reduction effect reaches 58.13% and the impact response spectrum is shown in Figure 16.

From the perspective of particle material, the impact reduction effect of iron based flexible boundary particle dampers is superior to other materials' flexible boundary particle dampers, and the effect is very obvious. Comparing the experimental results with the simulation results, as shown in Figure 17, it has been proven that the iron based particle flexible boundary particle damper has the optimal impact reduction effect.

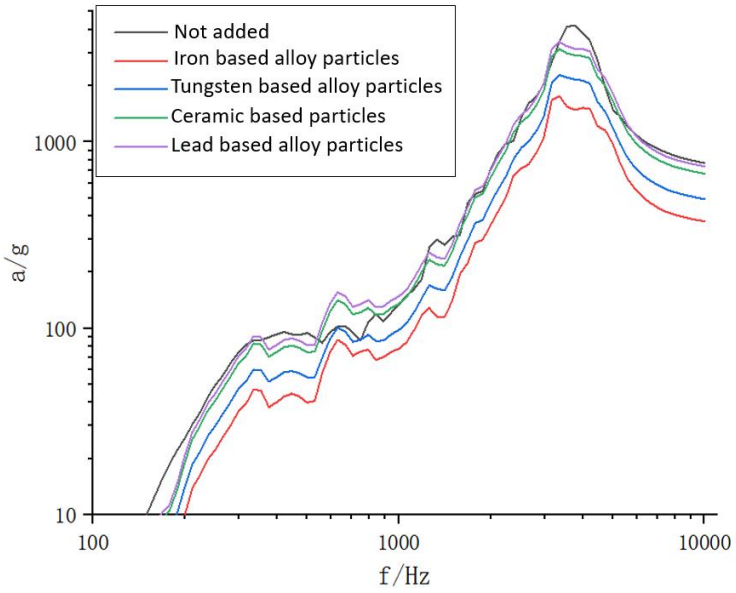

Figure 16. Impact response spectra of flexible boundary particle dampers with different materials installed.

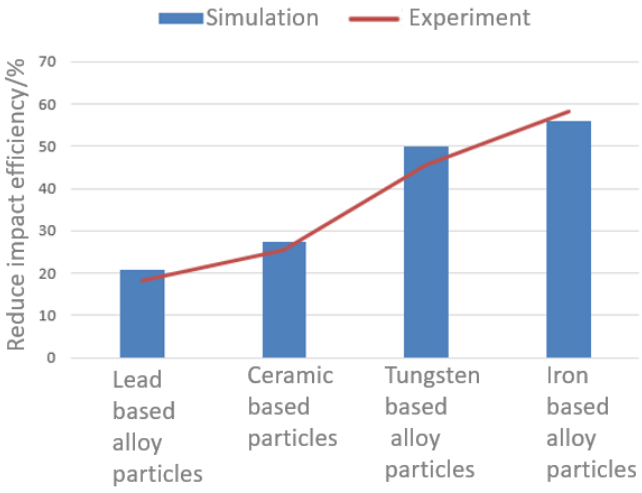

Figure 17. Comparison between experiment and simulation.

4.2. Verification of particle size

In this section, we investigate the influence of different particle sizes on the impact reduction effect of flexible boundary particle dampers. By filling a 30 mm wide flexible boundary particle damper inside the exposed platform and applying an impact load, dynamic response results are obtained at the target point where the precision instrument is located.

Three working conditions were designed for the experiment, and flexible boundary particle dampers with particle sizes of 1, 2 and 3mm were installed in the exposed platform. Impact experiments were conducted on the exposed platform to explore the influence of different particle sizes on the impact reduction effect of the flexible boundary particle damper. Among them, the other parameters of the flexible boundary particle damper are the same, the particle material is iron based alloy, the particle filling rate is selected as 95% and the thickness of the flexible boundary film is selected as 0.2 mm.

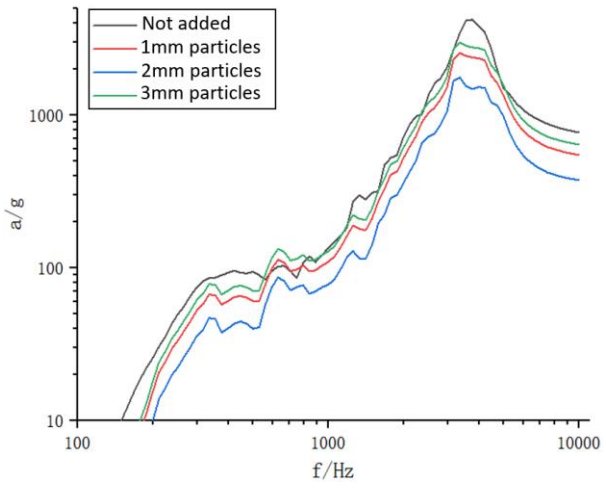

Figure 18. Impact response spectra of flexible boundary particle dampers with different particle sizes installed.

Through impact load excitation, it was measured that the maximum peak of the impact response spectrum of the exposed platform installed with a flexible boundary particle damper with a particle size of 1 mm appeared in the frequency range of 3000–4000Hz under impact excitation, with a maximum peak of 2546.52 g. Compared with the maximum peak of the impact response spectrum without a flexible boundary particle damper, the impact reduction effect reached 39.54%. The maximum peak value of the impact response spectrum of the exposed platform with a 2 mm particle size flexible boundary particle damper under impact excitation is 1763.53 g, which is 58.13% lower than the maximum peak value of the impact response spectrum without a flexible boundary particle damper installed. The maximum peak value of the impact response spectrum of the exposed platform with a flexible boundary particle damper with a particle size of 3mm under impact load excitation is 2977.4 g. Compared with the maximum peak value of the impact response spectrum without a flexible boundary particle damper, the impact reduction effect reaches 29.31%. The impact response spectrum is shown in Figure 18.

From the particle size perspective, the impact reduction effect of the iron based flexible boundary particle damper with a particle size of 2 mm is superior to that of other flexible boundary particle dampers, and the impact reduction effect is very obvious. Comparing the experimental results with the simulation results, as shown in Figure 19, it has been proven that the 2 mm iron based particle flexible boundary particle damper has the optimal impact reduction effect.

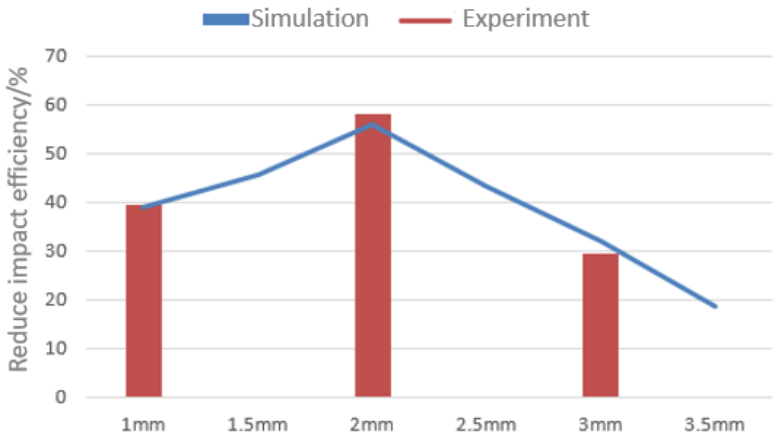

Figure 19. Comparison between experiment and simulation.

4.2. Pyrotechnic verification

Both pyrotechnic impact tests and light gas gun impacts can provide high-frequency, transient and high-order impact loads. However, pyrotechnic impact tests can simulate the most realistic spacecraft load environment. Therefore, pyrotechnic impact tests are used to ultimately verify the effectiveness of flexible boundary particle damping technology. The optimal characteristic parameters obtained from the impact experiment of the light gas gun, the flexible boundary damper, are applied to the exposed platform honeycomb panel for real pyrotechnic explosion experiments, and this is used as the final means to verify the impact reduction performance of the flexible boundary particle damping technology.

The exposed platform honeycomb panel is suspended in this pyrotechnics experiment, and a foam pad is placed at the bottom for support. The suspension frame and foam pad are shown in Figure 20(a).

The constraint method of the exposure platform for pyrotechnic experiments is shown in Figure 20(b). First, the exposed platform honeycomb panels without flexible boundary particle dampers were subjected to pyrotechnic explosion impact, and then the exposed platform honeycomb panels filled with flexible boundary particle dampers were subjected to pyrotechnic impact experiments to obtain the impact response spectra of both. The installation method of flexible boundary particle dampers is to install a 30 mm width around the ignition point, with 375 flexible boundary particle dampers filled and a total weight of approximately 1400 g. The particle material of the flexible boundary particle damper is iron based alloy, with a particle size of 2 mm and a filling rate of 95%. The flexible boundary film thickness is 0.2 mm. The packaging diagram of the flexible boundary particle damper is shown in Figure 20(c).

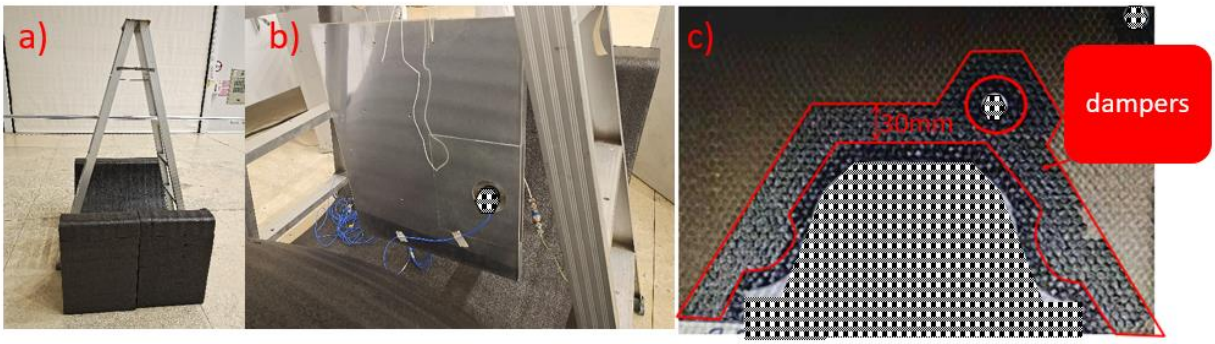

Figure 20. Construction and damper encapsulation of exposed honeycomb panel pyrotechnic experimental platform.

After completing the packaging of the flexible boundary particle damper and the assembly of the pyrotechnic separation device, measurement points were arranged at the exposed platform honeycomb board equipped with precision instruments. The overall experimental effect is shown in Figure 21(a), and the measurement points are shown in Figure 21(b).

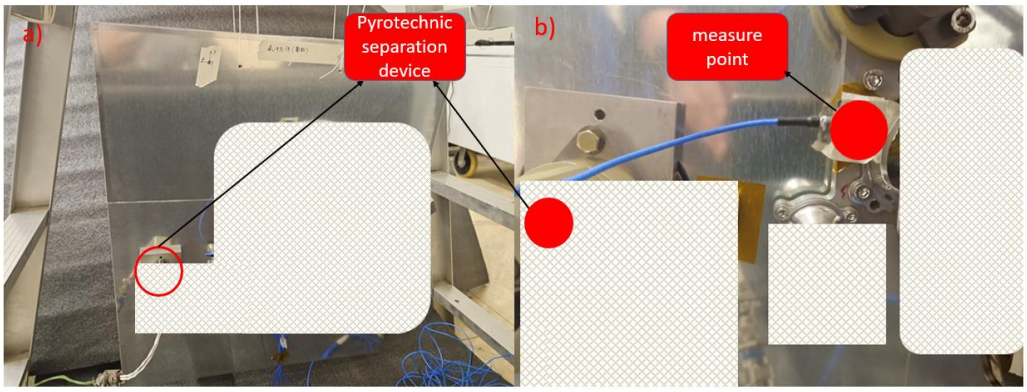

Figure 21. Installation and measurement points of honeycomb panels on exposed platforms.

In this chapter, we analyze the thermal shock response of exposed platform honeycomb panels without the installation of flexible boundary particle dampers and the exposed platform honeycomb panels with the optimal characteristic parameters of flexible boundary particle dampers. The final

shock response spectrum obtained from the experiment is shown in Figure 22.

According to the experimental results, it can be seen that the maximum peak value of the impact response spectrum is 6116.54 g when the honeycomb panel of the exposed platform is not equipped with a flexible boundary particle damper; When a flexible boundary particle damper with the optimal characteristic parameters is added to the honeycomb panel of the exposed platform, the maximum peak value of the impact response spectrum is 2720.25 g, and the impact reduction effect reaches 55.52%. The pyrotechnic experiment shows that the impact reduction effect of the flexible boundary particle damper with the optimal parameters is extremely significant.

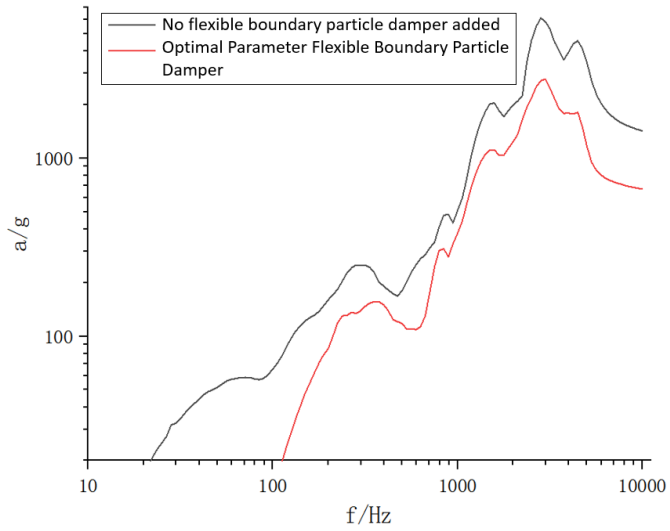

Figure 22. Impact response spectrum results of pyrotechnic experiment.

5. Conclusions

Using the exposed platform structure of the load compartment as the research subject, a flexible boundary particle damping system was designed to improve the dynamic characteristics of the exposed platform. After simulation calculation and experimental verification, the following conclusions can be drawn:

1) The simulation calculation results show that the use of iron based alloy particles in the flexible boundary particle damping system has a good impact reduction effect. The optimal particle size is 2 mm, the optimal filling rate is 95% and the optimal flexible boundary film thickness is 0.2 mm.

2) The results of the exposed platform impact test show that when the particle material is iron based alloy, the particle size is 2 mm, the filling rate is 95% and the boundary particle film thickness is 0.2 mm, the flexible boundary particle damper has the best impact reduction effect. The simulation calculation results are consistent with the trend of the impact reduction effect obtained from the impact test.

3) The results of the pyrotechnic impact test show that installing the flexible boundary particle damper with the optimal parameters on the exposed platform can achieve good impact reduction effect, effectively improving the impact response characteristics of the exposed platform and its impact reduction effect can reach 55.52%.

Use of AI tools declaration

The authors declare they have not used Artificial Intelligence (AI) tools in the creation of this article.

Acknowledgments

This work was supported by the National Natural Science Foundation of China [No.51875490]; Fujian Provincial Science and Technology Plan Project [No. 2022H6003]; Special fund project for basic scientific research business expenses of central universities [No.20720210042].

References

1. J. Lee, D. H. Hwang, J. H. Han, Study on Pyroshock propagation through plates with joints and washers, *Aerosp. Sci. Technol.*, **97** (2018), 441–458. https://doi.org/10.1016/j.ast.2018.05.057
2. H. Zhao, W. Liu, J. Ding, Y. Sun, X. Li, Y. Liu, Numerical study on separation shock characteristics of pyrotechnic separation nuts, *Acta Astronaut.*, **151** (2018), 893–903. https://doi.org/10.1016/j.actaastro.2018.07.040
3. J. Ding, H. Zhao, J. Wang, Y. Sun, Z. Chen, Numerical and experimental investigation on the shock mitigation of satellite-rocket separation, *Aerosp. Sci. Technol.*, **96** (2020), 105538. https://doi.org/10.1016/j.ast.2019.105538
4. D. H. Hwang, J. H. Han, J. Lee, Y. J. Lee, D. Kim, A mathematical model for the separation behavior of a split type low-shock separation bolt, *Acta Astronaut.*, **164** (2019), 393–406. https://doi.org/10.1016/j.actaastro.2019.07.035
5. X. Wang, Z. Qin, J. Ding, F. Chu, Finite element modeling and pyroshock response analysis of separation nuts, *Aerosp. Sci. Technol.*, **68** (2017), 380–390. https://doi.org/10.1016/j.ast.2017.05.028
6. A. García-Pérez, F. Sorribes-Palmer, G. Alonso, A. Ravanbakhsh, Overview and application of FEM methods for shock analysis in space instruments, *Aerosp. Sci. Technol.*, **80** (2018), 572–586. https://doi.org/10.1016/j.ast.2018.07.035
7. H. Zhao, Z. Hao, W. Liu, J. Ding, Y. Sun, Q. Zhang, et al., The shock environment prediction of satellite in the process of satellite-rocket separation, *Acta Astronaut.*, **159** (2019), 112–122. https://doi.org/10.1016/j.actaastro.2019.03.017
8. Q. Gong, J. Zhang, C. Tan, C. Wang, Neural networks combined with importance sampling techniques for reliability evaluation of explosive initiating device, *Chinese J. Aeronaut.*, **25** (2012), 208–215. https://doi.org/10.1016/S1000-9361(11)60380-4
9. J. R. Lee, C. C. Chia, C. W. Kong, Review of pyroshock wave measurement and simulation for space systems, *Measurement*, **45** (2012), 631–642. https://doi.org/10.1016/j.measurement.2011.12.011
10. V. Bateman, R. Merritt, Validation of pyroshock data, *J. IEST*, **55** (2012), 40–56. https://doi.org/10.17764/jiet.55.1.2q4650xqt7j0k506
11. W. Xiao, D. Lu, L. Song, H. Guo, Z. Yang, Influence of particle damping on ride comfort of mining dump truck, *Mech. Syst. Signal Process.*, **136** (2020), 106509. https://doi.org/10.1016/j.ymssp.2019.106509

12. W. Xiao, Z. Xu, H. Bian, Z. Li, Lightweight heavy-duty CNC horizontal lathe based on particle damping materials, *Mech. Syst. Signal Process.*, **147** (2021), 107127. https://doi.org/10.1016/j.ymssp.2020.107127
13. Z. Lu, K. Li, Y. Zhou, Comparative studies on structures with a tuned mass damper and a particle damper, *J. Aerosp. Eng.*, **31** (2018). https://doi.org/10.1061/(ASCE)AS.1943-5525.0000878
14. C. D. Johnson, P. S. Wilke, S. C. Pendleton, Softride vibration and shock isolation systems that protect spacecraft from launch dynamic environments, in *Proceedings of the 38th Aerospace Mechanisms Symposium*, (2006), 17–19.
15. T. Irvine, An introduction to the shock response spectrum, *Rev. P Vib.*, 2002.
16. J. G. Garcia, J. Albus, C. Hude, Isolation of sensible instrumentation-platforms against very highpyrotechnic shock in launch vehicles, in *ZProc of 52nd International Astronautical Congress*, 2001.
17. J. C. Yu, J. T. Wang, J. W. Pan, N. Guo, C. H. Zhang, A dynamic FEM-DEM multiscale modeling approach for concrete structures, *Eng. Fracture Mech.*, **278** (2023), 109031. https://doi.org/10.1016/j.engfracmech.2022.109031
18. W. Xiao, Y. Huang, H. Jiang, L. Jin, Effect of powder material on vibration reduction of gear system in centrifugal field, *Powder Technol.*, **294** (2016), 146–158. https://doi.org/10.1016/j.powtec.2016.01.038
19. M. Alkalla, X. Pang, C. Pitcher, Y. Gao, DROD: A hybrid biomimetic undulatory and reciprocatory drill: Quantitative analysis and numerical study, *Acta Astronaut.*, **182** (2021), 131–143. https://doi.org/10.1016/j.actaastro.2021.02.007
20. A. Tsarau, R. Lubbad, S. Løset, A numerical model for simulating the effect of propeller flow in ice management, **142** (2017), 139–152. https://doi.org/10.1016/j.coldregions.2016.06.002
21. W. Xiao, Z. Chen, T. Pan, J. Li, Research on the impact of surface properties of particle on damping effect in gear transmission under high speed and heavy load, *Mech. Syst. Signal Process.*, **98** (2018), 1116–1131. https://doi.org/10.1016/j.ymssp.2017.05.021
22. Y. Feng, J. Wu, C. Guo, B. Lin, Numerical simulation and experiment on excavating resistance of an electric cable shovel based on EDEM-RecurDyn bidirectional coupling, *Machines*, **10** (2022), 1203. https://doi.org/10.3390/machines10121203
23. W. Xiao, J. Li, S. Wang, X. Fang, Study on vibration suppression based on particle damping in centrifugal field of gear transmission, *J. Sound Vibration*, **366** (2016), 62–80. https://doi.org/10.1016/j.jsv.2015.12.014

AIMS Press